

52. R. P. Sharp, M. C. Malin, *Geol. Soc. Am. Bull.* **86**, 593 (1975).
53. D. C. Pieri, *Icarus* **27**, 25 (1976).
54. M. C. Malin, M. H. Carr, *Nature* **397**, 589 (1999).
55. M. H. Carr, M. C. Malin, *Icarus* **146**, 366 (2000).
56. D. L. Blaney, T. B. McCord, *J. Geophys. Res.* **94**, 10159 (1989).
57. P. R. Christensen *et al.*, *Science* **279**, 1692 (1998).
58. J. R. Zimbelman, *Lunar Planet. Sci.* **XXI**, 1375 (1990).
59. R. B. Leighton *et al.*, *Science* **149**, 627 (1965).
60. E. J. Öpik, *Ir. Astron. J.* **7**, 473 (1965).
61. W. K. Hartmann, *Icarus* **5**, 565 (1966).
62. ———, *Icarus* **15**, 410 (1971).
63. C. R. Chapman *et al.*, *Astron. J.* **74**, 1039 (1968).
64. L. A. Soderblom *et al.*, *Icarus* **22**, 239 (1974).
65. W. K. Hartmann, *J. Geophys. Res.* **78**, 4096 (1973).
66. K. L. Jones, *J. Geophys. Res.* **79**, 3917 (1974).
67. C. R. Chapman, *Icarus* **22**, 272 (1974).
68. R. A. Craddock, T. A. Maxwell, *J. Geophys. Res.* **95**, 14265 (1990).
69. ———, *J. Geophys. Res.* **98**, 3453 (1993).
70. Malin (84) considered the oldest terrain on Mars as cratered "volumes" rather than as cratered "surfaces," with craters formed over a period of time while deposition was occurring simultaneously. In such locations, the rim relief of a large crater might stick up through several younger layers, whereas some nearby smaller craters of comparable age might be buried, others might be exhumed, and still others, substantially younger than any of their neighbors, might also be visible.
71. M. C. Malin *et al.*, *Science* **279**, 1681 (1998).
72. M. C. Malin, K. S. Edgett, *Fifth International Conference on Mars* (abstr. 6027) (Lunar and Planetary Institute, Houston, TX, 1999) [CD-ROM].
73. R. B. Leighton, B. C. Murray, *Science* **153**, 136 (1966).
74. F. P. Fanale, *Icarus* **28**, 179 (1976).
75. Such variations have most often been invoked as the explanation for the repetitively layered polar materials.
76. W. R. Ward, *J. Geophys. Res.* **79**, 3375 (1974).
77. ——— *et al.*, *J. Geophys. Res.* **79**, 3387 (1974).
78. O. B. Toon *et al.*, *Icarus* **44**, 552 (1980).
79. M. C. Malin *et al.*, *J. Geophys. Res.* **97**, 7699 (1992).
80. W. K. Hartmann, *Meteorit. Planet. Sci.* **34**, 167 (1999).
81. G. Neukum, D. U. Wise, *Science* **194**, 1381 (1976).
82. G. Neukum, K. Hiller, *J. Geophys. Res.* **86**, 3097 (1981).
83. W. K. Hartmann *et al.*, in *Basaltic Volcanism on the Terrestrial Planets* (Pergamon, New York, 1981), pp. 1050–1129.
84. M. C. Malin, thesis, California Institute of Technology, Pasadena (1976), chap. 3.
85. J. A. Cutts, *J. Geophys. Res.* **78**, 4231 (1973).
86. D. H. Scott, K. L. Tanaka, *U.S. Geol. Surv. Misc. Inv. Ser. Map I-1802-A* (1986).
87. K. R. Blasius *et al.*, *J. Geophys. Res.* **82**, 4067 (1977).
88. K. L. Tanaka, M. G. Chapman, *Proc. Lunar Planet. Sci.* **22**, 73 (1992).
89. K. S. Edgett, T. J. Parker, *Geophys. Res. Lett.* **24**, 2897 (1997).
90. P. R. Christensen, *J. Geophys. Res.* **91**, 496 (1986).
91. ———, *J. Geophys. Res.* **93**, 7611 (1988).
92. E. M. Shoemaker, R. J. Hackman, in *The Moon: Symposium 14*, Z. Kopal, Z. K. Mikhailov, Eds. (Academic Press, New York, 1962), pp. 289–300.
93. D. E. Wilhelms, in *Planetary Mapping*, R. Greeley, R. M. Batson, Eds. (Cambridge Univ. Press, New York, 1990), pp. 208–260.
94. A. S. Selivanov *et al.*, *Nature* **341**, 593 (1989).
95. M. T. Mellon *et al.*, *Icarus*, in press.
96. W. K. Hartmann *et al.*, *Nature* **397**, 586 (1999).
97. W. K. Hartmann, D. C. Berman, *J. Geophys. Res.* **105**, 15011 (2000).
98. B. K. Lucchitta *et al.*, in *Mars*, H. H. Kieffer *et al.*, Eds. (Univ. of Arizona Press, Tucson, AZ, 1992), pp. 453–492.
99. R. V. Fisher, H.-U. Schmincke, *Pyroclastic Rocks* (Springer-Verlag, Berlin, 1984).
100. L. Keszthelyi, *et al.*, *J. Geophys. Res.* **105**, 15027 (2000).
101. We thank J. Garvin for assistance with laser altimeter data and thoughtful input from two anonymous referees. We thank D. Michna, M. Caplinger, E. Jensen, S. Davis, W. Gross, K. Supulver, J. Warren, R. Adair, J. Sandoval, L. Posiolov, R. Zimdar, and M. Ravine for operational support; we also express our appreciation to the MOC Science Team for their patience. Supported by the National Aeronautics and Space Administration through contract 959060 from the Jet Propulsion Laboratory.

25 September 2000; accepted 13 November 2000

## REPORTS

## Planar Hexacoordinate Carbon: A Viable Possibility

Kai Exner and Paul von Ragué Schleyer\*

The viability of molecules with planar hexacoordinate carbon atoms is demonstrated by density-functional theory (DFT) calculations for  $\text{C}_6\text{B}_6^{2-}$ , a  $\text{C}_6\text{H}_2$  isomer, and three  $\text{C}_3\text{B}_4$  minima. All of these species have six  $\pi$  electrons and are aromatic. Although other  $\text{C}_3\text{B}_4$  isomers are lower in energy, the activation barriers for the rearrangements of the three planar carbon  $\text{C}_3\text{B}_4$  minima into more stable isomers are appreciable, and experimental observation should be possible. High-level ab initio calculations confirm the DFT results. The planar hexacoordination in these species does not violate the octet rule because six partial bonds to the central carbons are involved.

Saturated carbon is usually tetrahedrally coordinated, and planar arrangements were long thought to be too high in energy to be observed. Nevertheless, experimental evidence for planar tetracoordinate carbon species predicted by theory (1–5) continues to accumulate (3, 6–9). Nonetheless, planar arrangements with six atoms bound to carbon seem impossible. Many known compounds have hexacoordinate carbons (Fig. 1) (10–18), but they are involved in three-dimensional structures.

Are planar hexacoordinate arrangements really inconceivable? The design of unusual

molecular shapes requires the right "fit" of the constituent atoms, both geometrically and electronically (3). The interatomic distances must be in the normal ranges. The molecular orbital (MO) patterns and degeneracies should be consistent with the molecular symmetry. In addition, the occupied orbitals should be low in energy and doubly occupied (1, 3, 19). Unusually high coordination of a central atom can best be achieved in cyclic systems or clusters in which all atom-atom contacts are bonding.

Our interest in planar hexacoordinate carbon was triggered by nucleus-independent chemical shift (NICS) evaluations of aromaticity (20–22). NICS values are based on magnetic shieldings computed by means of "ghost atoms" (designated points in space) positioned, for example, in the center of the

benzene ring. We wondered whether such surrogate probes could be replaced by a carbon atom or ion. If the cyclic electron delocalization is retained, the aromatic stabilization energy might help support unusual coordination of the central carbon. We now report an exploration of several candidates with carbon in the center of a six-membered ring using density-functional theory (DFT) calculations (B3LYP/6-311+G\*\*) (23).

It is not surprising that neutral atoms do not fit in the center of benzene. Very high energy (244 kcal mol<sup>-1</sup>) is needed to force helium (the smallest atom) to pass through the benzene plane [ $\text{He}@\text{C}_6\text{H}_6$  with hexagonal planar geometry ( $D_{6h}$  symmetry) is a transition state with bond lengths  $r_{\text{CC}} = r_{\text{CHe}} = 1.517 \text{ \AA}$ ]. The situation with a central carbon is even worse because the larger atomic radius and its excess valence electrons are unsupportable. Indeed, we could not optimize neutral  $\text{C}_7\text{H}_6$  when  $D_{6h}$  symmetry was imposed; even the Jahn-Teller-distorted  $D_{2h}$  form (9) (Fig. 2) was highly unstable, having 11 imaginary frequencies (an equilibrium structure has none) (24).  $D_{6h}$  optimization was possible after the removal of two electrons. The resulting  $\text{C}_7\text{H}_6^{2+}$  dication has a structure with 1.601 Å carbon-carbon bond lengths, but there are eight imaginary frequencies. The  $D_{6h}$  tetracation  $\text{C}_7\text{H}_6^{4+}$  (10), which can be imagined as a valence electron-stripped carbon atom inserted into benzene, has more realistic carbon-carbon bond lengths ( $r_{\text{CC}} = 1.516 \text{ \AA}$ ), but it is still characterized by two imaginary frequencies. The

Center for Computational Quantum Chemistry, Computational Chemistry Annex, University of Georgia, Athens, GA 30602–2525, USA.

\*To whom correspondence should be addressed. E-mail: schleyer@chem.uga.edu

high molecular charge leads to dissociation when symmetry restrictions are released. The isoelectronic boron analog  $\text{CB}_6\text{H}_6^{2-}$  (**11**), with seven imaginary frequencies, is even worse.

"Naked" clusters (that is, without hydrogens or other groups attached to the constituent atoms) are inherently better suited to stabilize central atom placements (3). For example, consider  $(\text{CH})_6$  (benzene) and  $\text{C}_6$  in

$D_{6h}$  symmetry. In benzene, the carbon in-plane orbitals are used to bind the hydrogens, but this valence capacity is underutilized in  $D_{6h}$   $\text{C}_6$ ; with the hydrogens stripped away,  $D_{3h}$  distortion results (25). Indeed,  $D_{6h}$   $\text{C}_7^{4+}$  (**12**) is characterized by only one imaginary frequency (24) of  $506.3i \text{ cm}^{-1}$ . But, the lengths of the partial carbon-carbon bonds to the central carbon (1.454 Å) are too short, and pyramidal distortion is favored.

We reasoned that replacement of the perimeter carbon atoms in **12** by boron atoms would result in a better "fit," because boron-carbon and boron-boron bond lengths are inherently longer than carbon-carbon bond lengths (26). Indeed, our DFT calculations show that the sixfold symmetric dianion  $\text{CB}_6^{2-}$  (**13**, isoelectronic with **12**) is a minimum [ $\nu_1 = 270.0 \text{ cm}^{-1}$ ; in this report,  $\nu_1$  denotes the lowest real frequency for minima and the largest imaginary frequency for structures where the number of imaginary frequencies (NIMAG) is greater than 1 (24)].

Why is **13**, the first minimum to be discovered with a planar hexacoordinate carbon, favorable? The MO plots for **13** (Fig. 3) reveal that no unfavorable orbitals are populated. The highest occupied orbitals are a degenerate  $\pi$  set ( $e_{1g}$ )

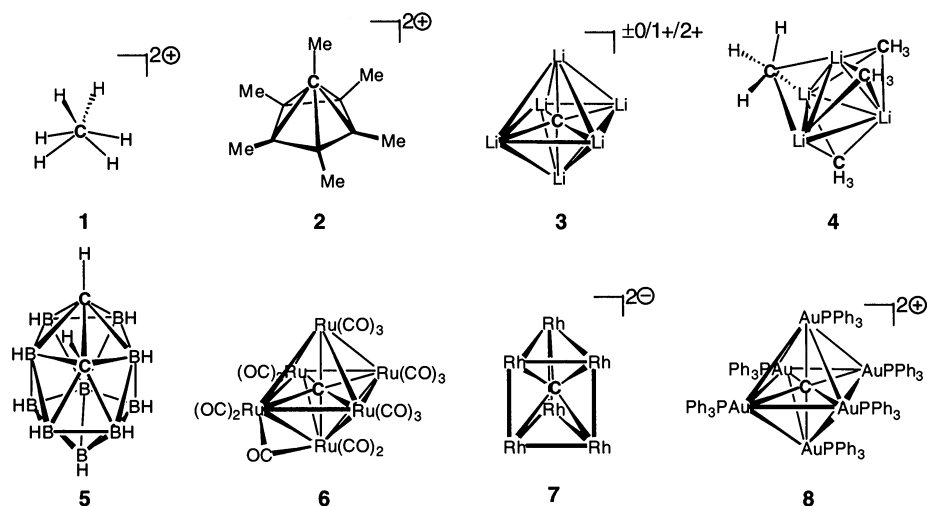
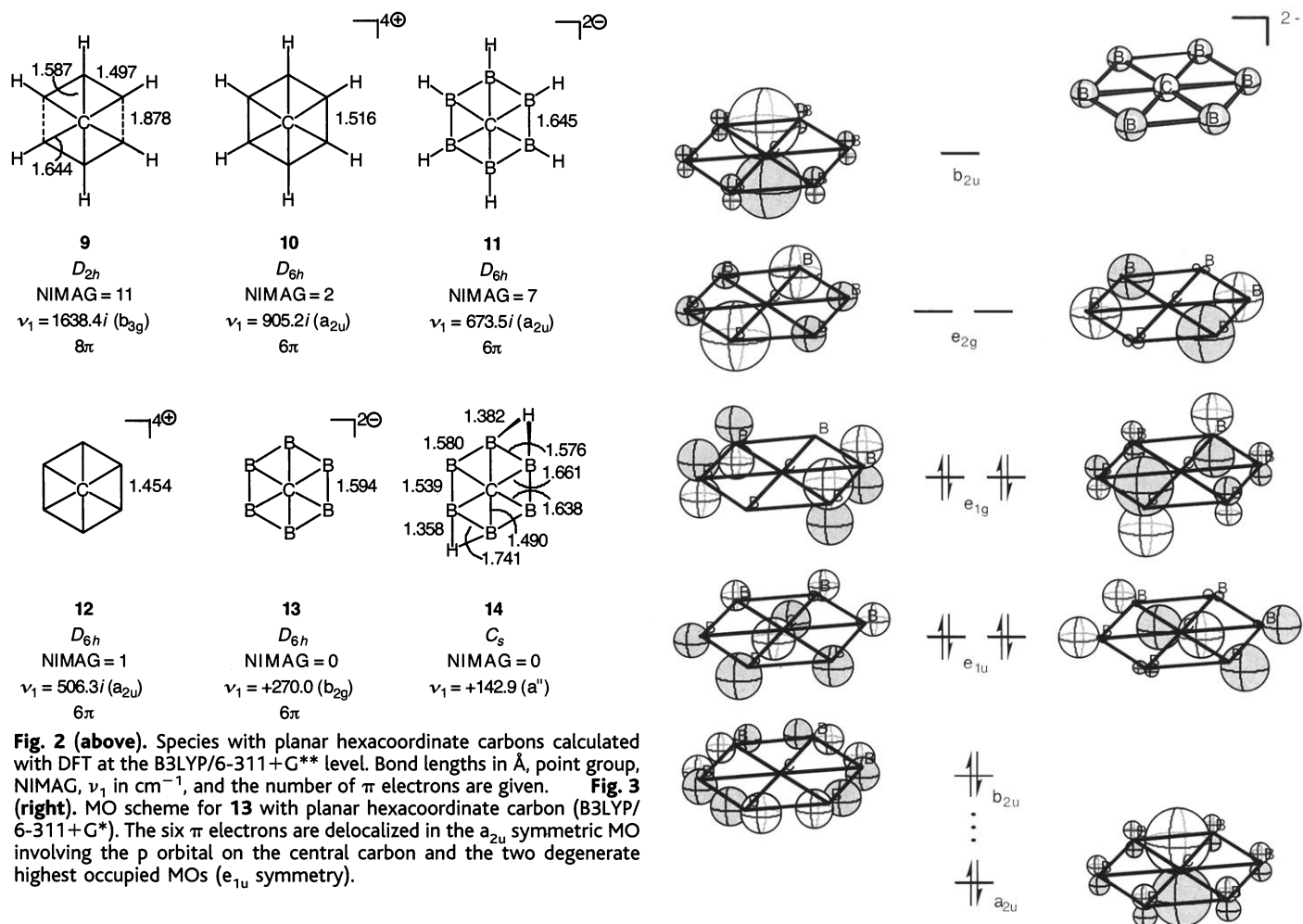


**Fig. 1.** Some compounds with hexacoordinate carbons:  $\text{CH}_6^{2+}$  (**1**) (14); Hogeveen's dication  $(\text{CCH}_3)_6$  (**2**) (12);  $\text{CLi}_6^{\pm 0/1+/2+}$  (**3**) (13, 15, 17); tetrameric MeLi (**4**); *ortho*- (**5**), *meta*-, and *para*- $\text{C}_2\text{B}_{10}\text{H}_{12}$ ;  $\text{CRu}_6(\text{CO})_{17}$  (**6**) (10);  $\text{CRh}_6(\text{CO})_{15}^{2-}$  (**7**) (CO ligands omitted for clarity) (11); and Schmidbaur's  $\text{C}[\text{Au}(\text{PPh}_3)_6]^{2+}$  (**8**) (16, 18).



just like those in benzene. The third occupied  $\pi$  MO, involving the p orbital at the central carbon ( $a_{2u}$  symmetry), is low in energy. Indeed, the sole 1.594 Å bond length computed in **13** is longer than the standard value for a carbon-boron single bond but is between the lengths of boron-boron single and double bonds (26). The Wiberg bond indices (WBI) (a measure of the bond order based on natural bond orbital analysis) quantify the nature of the bonding (27). As in the three-dimensional hexacoordinate carbon species (Fig. 1), the octet rule is not violated by the central carbon in **13**: partial bonds (WBI 0.63) to the six boron atoms are involved. The boron-boron WBI (1.29) is greater than 1.0 because of the aromatic  $6\pi$  electron character of the molecule (28). Therefore, **13** fulfills both the electronic and the geometrical requirements for good bonding (29).

We next tested whether neutral, closed-shell carbon-boron systems with planar hexacoordinate carbon are possible as well. All of the heavier atoms and one of the bridging hydrogens in the doubly protonated  $CB_6H_2$  minimum **14** lie very nearly in a plane. But, this is not the case for the second hydrogen; hence, the structure is not perfectly planar. We therefore pursued other design strategies. Isoelectronic substitution of carbon for boron in  $CB_6^{2-}$  (**13**, or boron for carbon in **12**) was successful: all three of the  $C_3B_4$  isomers with planar hexacoordinate carbons (**15** through **17**) are minima (Fig. 4).

The lowest frequencies of **15** through **17** are appreciable in magnitude ( $>150\text{ cm}^{-1}$ ) (Fig. 4) and, like those of **13** and **14**, are associated with movement of the central hexacoordinate carbon in **15** through **17** out of the ring plane. But, unlike **12**, where this out-of-plane motion is favorable, the  $C_3B_4$  structures (**15** through **17**) have optimal bond lengths. In addition, the orbital interactions of

the central carbon atoms with the  $C_2B_4$  perimeter stabilize the unprecedented bonding patterns. As with **13** (Fig. 3), no unfavorable orbitals are populated in any of the **15** through **17** isomers, all of which are aromatic as a result of their six cyclically delocalized  $\pi$  electrons (28). Consequently, the WBI of the partial bonds to the central carbons are substantial (Fig. 4).

The predicted existence of compounds with a planar hexacoordinate carbon is exciting, but there is still a question as to whether isomers **15** through **17** are viable. These minima do have appreciably positive lowest vibrational frequencies ( $>150\text{ cm}^{-1}$ ), but this criterion is only a necessary, not a sufficient, prerequisite for their observation: rearrangements to more stable  $C_3B_4$  isomers must not take place on the time scale of the method of detection. An extensive search of the  $C_3B_4$  hypersurface through geometry optimizations, first at the B3LYP/6-31G\* and then at the B3LYP/6-311+G\* levels, followed by frequency analyses, identified 16 additional minima [see Web fig. 1 (30) and Fig. 5]. Thirteen of these minima are more stable than **15** through **17**, but the lowest rearrangement barriers are appreciable: **15**  $\rightarrow$  **18** (34.4 kcal mol $^{-1}$ ), **16**  $\rightarrow$  **19** (25.8 kcal mol $^{-1}$ ), and **17**  $\rightarrow$  **20** (19.1 kcal mol $^{-1}$ ) (31).

Are those energies reliable? The DFT method applied is known to give accurate geometries, but it sometimes overestimates activation barriers. We therefore performed CCSD(T)/cc-pVTZ single-point calculations for **15** through **17** and the corresponding transition states to get accurate energies. The relative energies for **15** through **17** at the CCSD(T) level are 11.9 (**15**), 0.0 (**16**), and 6.2 kcal mol $^{-1}$  (**17**), in good agreement with the DFT energies (12.4, 0.0, and 6.0 kcal mol $^{-1}$ , respectively). The T1 diagnostics (32) (all less than the 0.02 threshold value) indi-

cate that **15** through **17** are well described by a single electronic configuration. The activation energies of 34.5 (**15**), 31.0 (**16**), and 22.5 kcal mol $^{-1}$  (**17**) also support the DFT values. The T1 diagnostics (0.039, 0.032, and 0.040, respectively) indicate some multireference character of the transition states (33).

We conclude that molecules with planar hexacoordinate carbon are possible. Although the first examples (**13** through **17**) of this novel bonding motive can rearrange to more stable isomers, the barriers should be sufficiently high to permit observation, particularly of **15** (34). Fragmentation and (auto)ionization of these compounds require high energy. Dimerization or the formation of even higher aggregates may be possible, but the isolated species with planar hexacoordinate carbon should be viable in the gas phase (3) or in a matrix. Further examples, more amenable to experimental characterization, may be found in larger mixed-element clusters. As with planar tetracoordinate carbon (1–9) and nonplanar hexacoordinate carbon species (10–18), our findings further extend the traditional view of the bonding capabilities of carbon and, by implication, other main group elements.

#### References and Notes

- R. Hoffmann, R. W. Alder, Ch. F. Wilcox, *J. Am. Chem. Soc.* **92**, 4992 (1970).
- J. B. Collins et al., *J. Am. Chem. Soc.* **98**, 5419 (1976).
- P. v. R. Schleyer, A. I. Boldyrev, *J. Chem. Soc. Chem. Commun.* **1991**, 1536 (1991). The prediction in this paper that molecules like  $CaI_2Si_2$  would have planar tetracoordinate carbons has been verified experimentally by the detection of the isoelectronic  $CaI_3Si^-$  species [L.-S. Wang, A. I. Boldyrev, X. Li, J. Simons, *J. Am. Chem. Soc.* **122**, 7681 (2000)].
- K. Sorger, P. v. R. Schleyer, *J. Mol. Struct. Theochem* **338**, 317 (1995).
- L. Radom, D. R. Rasmussen, *Pure Appl. Chem.* **70**, 1977 (1998).
- W. Siebert, A. Gunale, *Chem. Soc. Rev.* **28**, 367 (1999).
- D. Röttger, G. Erker, *Angew. Chem. Int. Ed. Engl.* **36**, 813 (1997).
- R. Choukroun, P. Cassoux, *Acc. Chem. Res.* **32**, 494 (1999).
- X. Li, L. S. Wang, A. I. Boldyrev, J. Simons, *J. Am. Chem. Soc.* **121**, 6033 (1999).
- A. Sirigu, M. Bianchi, E. Benedetti, *J. Chem. Soc. Chem. Commun.* **1969**, 596 (1969).
- V. G. Albano, M. Sansoni, P. Chini, S. Matinego, *J. Chem. Soc. Dalton Trans.* **1973**, 651 (1973).
- H. Hogeveen, P. W. Kwant, *Acc. Chem. Res.* **8**, 413 (1975).
- E. D. Jemmis, J. Chandrasekhar, E.-U. Würthwein, P. v. R. Schleyer, *J. Am. Chem. Soc.* **104**, 4275 (1982).
- K. Lammertsma et al., *J. Am. Chem. Soc.* **105**, 5258 (1983).
- P. v. R. Schleyer, E.-U. Würthwein, E. Kaufmann, T. Clark, J. A. Pople, *J. Am. Chem. Soc.* **105**, 5930 (1983).
- F. Scherbaum, A. Grohmann, G. Müller, H. Schmidbaur, *Angew. Chem. Int. Ed. Engl.* **28**, 463 (1989).
- P. v. R. Schleyer, J. Kapp, *Chem. Phys. Lett.* **255**, 363 (1996).
- F. P. Gabbai, A. Schier, J. Riede, H. Schmidbaur, *Chem. Ber. Recl.* **130**, 111 (1997).
- A. I. Boldyrev, J. Simons, *J. Am. Chem. Soc.* **120**, 7967 (1998).
- P. v. R. Schleyer, C. Maerker, A. Dransfeld, H. J. Jiao, N. Hommes, *J. Am. Chem. Soc.* **118**, 6317 (1996).
- P. v. R. Schleyer, H. Jiao, N. J. R. van Eikema Hommes,

**Fig. 4.** Stable neutral  $C_3B_4$  minima with a planar hexacoordinate carbon atom (B3LYP/6-311+G\*). Bond lengths in Å, WBI (in italics), point group, NIMAG, lowest real frequency ( $\nu_1$ ) in  $\text{cm}^{-1}$ , the number of  $\pi$  electrons, and the zero-point corrected relative energy ( $E_{\text{Orel}}$ ) in kcal mol $^{-1}$  are given.

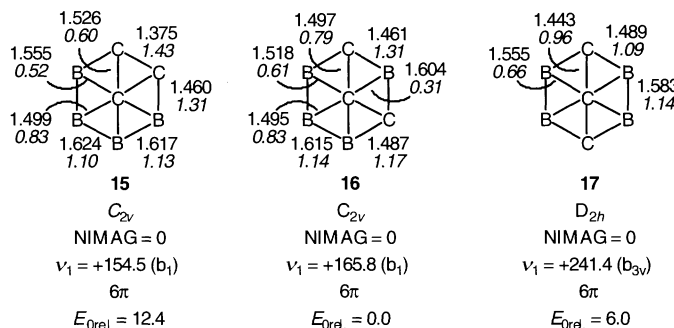
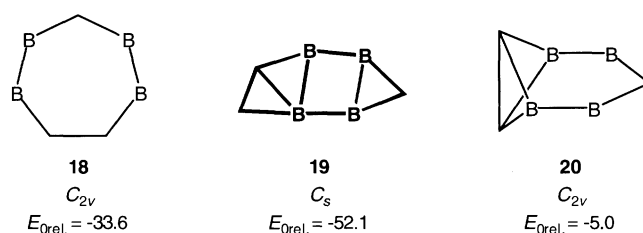


**Fig. 5.** Primary isomerization products of **15** through **17** (B3LYP/6-311+G\*). The zero-point corrected energies in kcal mol $^{-1}$  are relative to **16**.



# Geodynamic Evidence for a Chemically Depleted Continental Tectosphere

Alessandro M. Forte\* and H. K. Claire Perry

The tectosphere, namely the portions of Earth's mantle lying below cratons, has a thermochemical structure that differs from average suboceanic mantle. The tectosphere is thought to be depleted in its basaltic components and to have an intrinsic buoyancy that balances the mass increase associated with its colder temperature relative to suboceanic mantle. Inversions of a large set of geodynamic data related to mantle convection, using tomography-based mantle flow models, indicate that the tectosphere is chemically depleted and relatively cold to 250 kilometers depth below Earth's surface. The approximate equilibrium between thermal and chemical buoyancy contributes to cratonic stability over geological time.

The tectosphere refers to the mantle below continental lithosphere that is assumed to be stabilized against convective disruption by a balance between thermally generated negative buoyancy and positive chemical buoyancy (1, 2). Seismic, petrologic, and heat flow data have suggested that both the subcontinental chemical boundary layer (CBL) and thermal boundary layer (TBL) extend to about 200 km depth (3, 4). More recent studies based on continental heat flow and gravity data indicate that the tectosphere TBL extends to depths between 200 and 330 km (5, 6). Additional constraints on the thermochemical structure and depth extent of the tectosphere are provided by mantle xenolith data (7–9). The interpretation of heat flow and gravity data is, however, nonunique, and the xenolith data represent a limited sampling of the deep structure of the tectosphere.

High-resolution seismic tomography provides detailed reconstructions of the three-dimensional (3D) structure in the mantle (10–13). Tomographic models derived from short-period seismic surface waves (10, 13) provide optimal vertical resolution of the 3D structure in the tectosphere (14). These 3D models show a tectosphere characterized by sublithospheric shear wave speeds about 5% faster than shear wave speeds in the ambient mantle. A recent interpretation of this shear velocity heterogeneity suggests that the tectosphere TBL extends to a maximum depth of about 230 km, but a corresponding CBL was not detected (15). Shear velocity anomalies alone cannot distinguish chemical heterogeneity in the tectosphere, unless they are combined with constraints on the tectosphere density structure (16).

We derived constraints on the tectosphere

density structure using a reformulated mantle flow theory (17) that incorporates surface tectonic plates whose motions are coupled to the underlying mantle flow. In the flow modeling, we used two recent high-resolution models of seismic shear wave velocity heterogeneity (11, 13), which are derived from independent data, using different parameterizations of the heterogeneity and different inversion procedures. Constraints on mantle density anomalies, and consequently the thermochemical structure of the tectosphere, are then obtained by inverting convection-related geodynamic data with the mantle flow model.

The convection data we use are the tectonic plate velocities (18), the global free-air gravity anomalies (19), the surface topography corrected for crustal isostasy (20), and the excess or dynamic ellipticity of the core-mantle boundary (21, 22). These data provide independent constraints on mantle density, with different sensitivities to density anomalies at different depths (23). The surface topography (Fig. 1) provides the strongest constraint on density variations in the lithospheric mantle, and thus a number of tomography-based mantle flow studies have used surface topography to constrain the density structure and dynamics of the tectosphere (24–27).

We first estimated mantle density anomalies ( $\delta\rho$ ), which provide the buoyancy forces for mantle flow, from shear wave velocity anomalies ( $\delta V_s$ ) using a mineral physics estimate (28) of the velocity-to-density conversion  $d\ln\rho/d\ln V_s$ . Mantle flow modeling also requires a knowledge of mantle rheology, which we represent as a depth-dependent viscosity. We derived the mantle viscosity profile through nonlinear iterative inversions (17) of the convection data, using the initial estimate of  $\delta\rho$ . The viscosity profiles we obtained (Fig. 2A) are characterized by a low-viscosity zone at ~200 km depth.

The density structure of the tectosphere is

V. G. Malkin, O. L. Malkina, *J. Am. Chem. Soc.* **119**, 12669 (1997).

22. An extended bibliography of NICS values is given by S. Patchkovskii and W. Thiel [*J. Mol. Model.* **6**, 67 (2000)].
23. M. J. Frisch *et al.*, Gaussian 98 (Revision A.7) (Gaussian, Pittsburgh, PA, 1998).
24. An imaginary frequency indicates the existence of a vibrational mode that is dynamically unstable and leads to a more stable structure. Transition states of a chemical reaction are saddle points exhibiting only one imaginary frequency. Saddle points with more than one imaginary frequency may be visited by dynamical systems with sufficiently high vibrational energy but are generally not of chemical significance.
25. P. v. R. Schleyer, H. Jiao, M. N. Glukhovtsev, J. Chandrasekhar, E. Kraka, *J. Am. Chem. Soc.* **116**, 10129 (1994).
26. The typical carbon-carbon, carbon-boron, and boron-boron bond lengths (B3LYP/6-311+G\*\*) are as follows: H<sub>3</sub>C–CH<sub>3</sub> (*D<sub>3d</sub>*), 1.531 Å; H<sub>2</sub>C=CH<sub>2</sub> (*D<sub>2h</sub>*), 1.329 Å; H<sub>3</sub>C–BH<sub>2</sub> (*C<sub>s</sub>*), 1.554 Å; CH<sub>2</sub>=BH (*C<sub>2v</sub>*), 1.376 Å; H<sub>2</sub>B–BH<sub>2</sub> (*D<sub>2d</sub>*), 1.629 Å; and HB=BH (*D<sub>2h</sub>*), 1.523 Å.
27. Bonding was computed at B3LYP/6-31G\*/B3LYP/6-311+G\*. The Natural Bond Orbital (NBO) implementation in Gaussian 98 cannot handle CB<sub>6</sub><sup>2-</sup> at the B3LYP/6-311+G\* level (linear-dependent basis set).
28. The NICS values in parts per million (20–22) (B3LYP/6-311+G\*\*) 1.0/1.5 Å above the central carbons of **13** (–22.8/–9.7), **15** (–22.8/–10.2), **16** (–22.1/–9.9), and **17** (–23.6/–10.9) document the aromatic character of these hexacoordinate carbon species; the values above the center of benzene are –10.2/–7.6.
29. The concept of the right geometrical “fit” (3) is further demonstrated by species like NB<sub>6</sub><sup>–</sup>, PB<sub>6</sub><sup>–</sup>, OB<sub>6</sub>, and SB<sub>6</sub> with a cyclic B<sub>6</sub> ligand. These species are isoelectronic with D<sub>6h</sub> symmetrical CB<sub>6</sub><sup>2-</sup> (**13**), but NB<sub>6</sub><sup>–</sup> and SB<sub>6</sub> adopt *D<sub>2h</sub>* symmetry because of a “minor” bond-length mismatch (but still feature planar hexacoordinate nitrogen and oxygen). In contrast, phosphorous and sulfur are too large to fit into the B<sub>6</sub> ring. Consequently, C<sub>6v</sub> symmetric structures of PB<sub>6</sub><sup>–</sup> and SB<sub>6</sub> result, having the “coordinated” atoms positioned above the B<sub>6</sub> plane.
30. Supplemental material is available at [www.sciencemag.org/cgi/content/full/290/5498/1937/DC1](http://www.sciencemag.org/cgi/content/full/290/5498/1937/DC1).
31. Isomers **18** and **20** easily rearrange into **19** with barriers of 3.2 (**18** → **19**) and 8.9 kcal mol<sup>–1</sup> (**20** → **19**), respectively.
32. T. J. Lee, P. R. Taylor, *Int. J. Quant. Chem. Quant. Chem. Symp.* **23**, 199 (1989).
33. This multireference character was also shown and taken into account by CASSCF(6,10)/6-311+G\* calculations. The relative energies of **15** through **17** were reproduced well (13.3, 0.0, and 5.5 kcal mol<sup>–1</sup>, respectively). Although the activation barrier for the isomerization of **15** (33.1 kcal mol<sup>–1</sup>) was almost unchanged as compared to the B3LYP and CCSD(T) calculations, the barriers for **16** (8.5 kcal mol<sup>–1</sup>) and **17** (12.8 kcal mol<sup>–1</sup>) were smaller. CAS-MP2 runs with Gaussian 98 gave only “bizarre results,” as has been noted earlier for Gaussian 94 by Th. Bally and W. T. Borden [in *Reviews in Computational Chemistry*, K. B. Lipkowitz, D. B. Boyd, Eds. (Wiley, New York, 1999), vol. 13, footnote on p. 36].
34. Generation of the hexacoordinate carbon compounds by laser vaporization of a suitable target combined with instantaneous cooling of the generated molecules to ~4 K in a supersonic jet might allow subsequent matrix isolation and/or spectroscopic detection of these exciting species, even for **16** and **17** with their lower barriers for isomerization [compare work by V. E. Bondybey, A. M. Smith, and J. Argreiter [*Chem. Rev.* **96**, 2113 (1996)] and D. S. Perry and G. A. Bethardy [in *Techniques of Chemistry Series*, A. B. Myers, Th. R. Rizzo, Eds. (Wiley, New York, 1995), vol. XXIII, chap. 3]].
35. We thank H. Prinzbach, Freiburg, for his encouragement. This work was supported by the Fonds der Chemischen Industrie through a postdoctoral fellowship (K.E.).

19 June 2000; accepted 1 November 2000

Department of Earth Sciences, University of Western Ontario, London, Ontario N6A 5B7, Canada.

\*To whom correspondence should be addressed. E-mail: [aforte@uwo.ca](mailto:aforte@uwo.ca)